IIETA International Information and Engineering Technology Association
Advancing the World of Information and Engineering

Instrumentation Mesure Métrologie
Vol. 25, No. 3, June 2026, pp. 127-134
Journal homepage: http://iieta.org/journals/i2m

Design and Accuracy Assessments of a Low-Cost IoT-Based Tide Gauge for Hydrographic Surveying

Bandi Sasmito*, Hana Sugiastu Firdaus, Moehammad Awaluddin

Department of Geodetic Engineering, Faculty of Engineering, Diponegoro University, Semarang, Central Java 50275, Indonesia

Corresponding Author Email: bandisasmito@live.undip.ac.id

https://doi.org/10.18280/i2m.250304

Received: 2 April 2026
Revised: 9 June 2026
Accepted: 18 June 2026
Available online: 26 June 2026

Keywords:
Arduino, hydrographic surveying, Internet of Things, Automatic Water Level Recorder, vertical datum, IHO S-44

ABSTRACT

Accurate water-level monitoring is essential for establishing the vertical datum in hydrographic surveying and maritime engineering. However, the widespread deployment of industrial-grade Automatic Water Level Recorders (AWLRs) is often hindered by high procurement costs and limited portability. This research aims to design and evaluate the reliability of a cost-effective, highly portable Arduino-based AWLR utilizing an ultrasonic sensor and local data storage. To overcome remote field operational constraints, an innovative in-situ geodetic vertical calibration framework using optical levelling (auto level, locally called waterpass) was implemented to systematically tie the sensor's zero-reference point to the national vertical datum. Field validation was conducted over 48 hours at Kartini Beach, Jepara, benchmarking the instrument against manual tide staff observations and an industrial-grade automated reference station managed by the Geospatial Information Agency (BIG). To mitigate high-frequency environmental noise, a Simple Moving Average (SMA) statistical filter was applied. Comprehensive error budget decomposition showed that the SMA filter successfully compressed the random scatter (Standard Deviation (SD)) from ±6.3 cm to ±1.5 cm against the tide staff, and from ±2.4 cm to ±1.1 cm against the BIG station. The final filtered datasets demonstrated exceptional precision, yielding a Root Mean Square Error (RMSE) of 2.7 cm (Mean Bias Error (MBE) of +2.2 cm) against the manual tide staff, and a highly precise RMSE of 1.7 cm (MBE of +1.3 cm) against the automated BIG station. Signal fidelity analysis further confirmed zero artificial phase lag and negligible peak distortion (<0.1 cm). These findings conclusively confirm that the developed low-cost instrument satisfies the strict tidal reduction component of the Total Vertical Uncertainty (TVU) budget mandated by the International Hydrographic Organization (IHO) S-44 standards for Special Order and Order 1 hydrographic surveys. Consequently, this IoT-based tide gauge serves as a scientifically valid and reliable solution to complement professional hydrographic mapping, particularly in data-scarce or remote coastal regimes.

1. INTRODUCTION

Monitoring of water level elevation is a fundamental parameter in various earth disciplines, especially in the scope of hydrographic surveys, coastal area management, and maritime infrastructure engineering [1, 2]. In engineering surveys, precise tidal data are an absolute requirement for determining the vertical datum, which serves as the primary reference for bathymetric mapping, shipping channel planning, and flood disaster mitigation in coastal areas [3, 4]. Accuracy in these measurements is crucial, as errors in determining water level elevation can have fatal consequences on the design of civil engineering structures and the safety of marine navigation [5, 6]. As the need for real-time data increases, the transition from manual observation to automated systems is becoming a necessity in the modern geomatics industry.

Traditionally, tidal measurements are performed using an industry-standard Automatic Water Level Recorder (AWLR) instrument that offers high precision. However, the widespread implementation of these tools is often hampered by the high procurement costs and complex, permanent installation procedures [7, 8]. Limited flexibility and large tool dimensions result in an uneven distribution of tidal monitoring stations, especially at survey project locations that are temporary or in remote, difficult-to-reach areas [9, 10]. As a result, many engineering survey practitioners still rely on modeling or interpolating data from distant permanent stations, which can reduce the accuracy of local elevation data.

The development of open-source microcontroller technology and the Internet of Things (IoT) ecosystem provides a new paradigm for the development of low-cost yet effective environmental monitoring instruments [11, 12]. The use of platforms such as Arduino enables the integration of various digital sensors for independent, continuous data acquisition [13, 14]. Among the wide range of technology

options, ultrasonic sensors are among the most popular for distance measurement due to their non-contact nature, which makes them more resistant to seawater corrosion than contact-type sensors [15, 16]. In addition, pressure sensors are often used as alternatives or complements to improve measurement accuracy under certain environmental conditions [17].

Although the potential for developing IoT-based self-measuring tools is enormous, the main challenge from an engineering perspective is the reliability and consistency of the resulting data [18, 19]. The reliability of an instrument is not only judged by its technical ability to record data, but also its ability to provide stable results in the midst of environmental noise disturbances, such as wave ripples and air temperature fluctuations [20, 21]. Therefore, the application of statistical filtering methods, such as the Moving Average Algorithm, is crucial for reducing systematic errors and improving the quality of tidal data [22]. Validation of standard instruments and manual observation methods remains the standard for determining whether a prototype is suitable for professional use.

This study aims to design, build, and evaluate the reliability of an Arduino-based automatic tidal-measuring device specifically for portable hydrographic survey needs. The main focus of this study is to conduct a comparative analysis of data generated by the prototype device with manual observation data (tide staff) and official reference data from the Geospatial Information Agency (BIG) station located at Kartini Beach, Jepara Regency, Central Java, Indonesia. By integrating expertise in geodesy techniques and the latest sensor technology, this study is expected to provide technical recommendations for standardizing the use of low-cost instruments to meet spatial data needs in the scope of survey and hydrographic engineering.

2. METHODOLOGY

The research conducted in this study comprises tool design, field data acquisition, and analysis of the acquired results in the laboratory.

2.1 Instrument design

The Instrument is designed to measure water levels in the water by stringing sensors with an Arduino UNO at the center. Figure 1 shows a microcontroller from Arduino controlling several sensors.

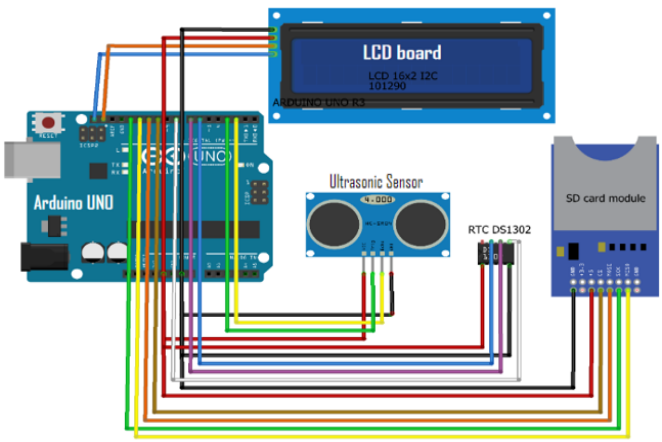

Figure 1. Arduino and sensor wiring diagram

The Arduino input/output (I/O) pins in Figure 1 are connected to several sensors and boards. The ultrasonic sensor measures distance. The Real Time Clock (RTC) board records time on the go. The Liquid Crystal Display (LCD) board is installed to show the setup and measurement results visually. An SD card is added to record and save measurement results into data. With the Arduino IDE, the Arduino board is programmed to work.

The operational workflow begins by instructing the ultrasonic sensor to transmit a beam of sound waves toward the water target and receive the reflected signal to calculate the time-of-flight distance. Simultaneously, the system requests the current time recorded by the RTC board. To optimize data density, the programming loop is throttled to record one distance measurement every 10 seconds. The acquired data is displayed on the LCD and concurrently written to the SD card memory for subsequent download and post-processing. Once the electrical system is validated, it is housed inside a rigid 3-inch Polyvinyl Chloride (PVC) pipe enclosure, which easily doubles as a wave-dampening system and allows for straightforward assembly and disassembly across temporary field locations.

Table 1. Bill of Materials (BOM) and hardware technical specifications

Component	Specification/Model	Operational Range/Parameters
Microcontroller	Arduino UNO (ATmega328P)	5 V operating voltage, 16 MHz
Ultrasonic Sensor	JSN-SR04T (Waterproof)	Range: 20 cm–600 cm; Blind Zone: 20 cm
Beam Angle	Transducer Cone	Approximately 45° to 60°
Data Storage & RTC	MicroSD Module + DS3231 RTC	SPI communication, I2C high-precision clock
Power Supply	Sealed Lead-Acid Battery	12 V regulated to 5 V via buck converter
Enclosure/Well	Rigid PVC Pipe	Diameter: 3 inches (Mechanical stilling well)

Note: RTC = Real Time Clock, SPI = Serial Peripheral Interface, I2C = Inter-Integrated Circuit, PVC = Polyvinyl Chloride (PVC).

Figure 2. Instruments installation, design and configuration

To ensure the instrument's performance under harsh marine conditions, the specific hardware components were carefully selected. The JSN-SR04T waterproof ultrasonic sensor was employed due to its proven resistance to humidity and salt spray typical of coastal environments. The sensor operates

with a 20 cm blind zone, a 600 cm maximum range, and a directional beam angle as shown in Table 1. Internal temperature compensation was handled natively by the code logic to mitigate the non-linear effects of varying ambient air temperatures on the velocity of sound. The overall tool body and the sensor mounting arm utilize lightweight PVC components to facilitate rapid deployment (Figure 2). The complete microcontrollers, circuits, and batteries are sealed within the upper waterproof PVC compartment to protect against splashing waves, as structurally schematized in Figure 3.

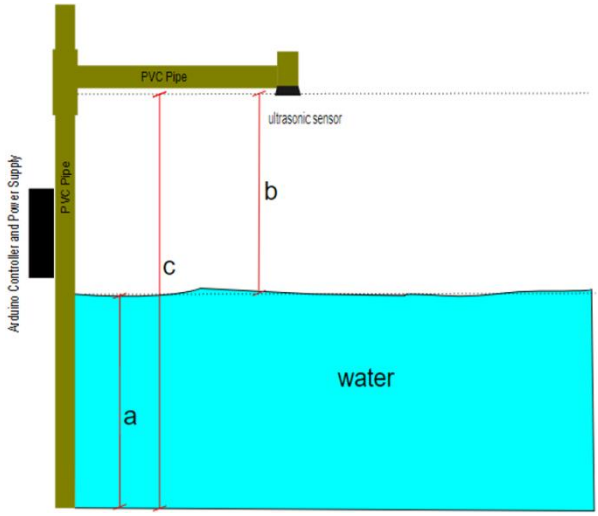

Figure 3. Tool configuration design during data acquisition

The localized tidal water level is calculated by subtracting the measured sensor distance from the established installation height relative to the reference zero-datum, expressed as Eq. (1).

$$a = c - b \tag{1}$$

where, a is the computed instantaneous water level (tide height), b is the distance recorded by the ultrasonic sensor, and c is the absolute height of the sensor transducer relative to the bottom benchmark, predetermined via an auto-level geodetic instrument. The schematic configuration of this design is illustrated in Figure 3, while the actual continuous field deployment setup at Kartini Beach is shown in Figure 4.

2.2 In-situ calibration and geodetic vertical alignment

Field deployment and experimental testing were conducted adjacent to an official reference tidal station at Kartini Beach, Jepara Regency, Central Java, Indonesia (Station Code: JPRA, located at 06°35'29.54" S, 110°38'55.32" E), as illustrated in Figure 4. Continuous manual tidal observations were recorded simultaneously using a standard physical tide staff to establish a baseline validation dataset.

Due to remote field operational constraints, a static laboratory calibration bench was bypassed; instead, a rigorous and reproducible in-situ geometric calibration and validation framework was implemented during the initial deployment phase. The primary methodological novelty of this work does not merely lie in the low-cost hardware assembly, but rather in the systematic integration of high-precision geodetic optical levelling directly into the low-cost instrument's calibration chain. The zero-reference point of the ultrasonic transducer was physically and mathematically tied to the local vertical datum reference via direct optical alignment with the manual tide staff shown in Figure 5.

Figure 4. Installation at the test station site

Figure 5. Point of view for height reference

Furthermore, to verify the linearity and stability of the sensor's acoustic response across the dynamic tidal range, continuous baseline observations were verified against the tide staff during the critical highest and lowest slack water periods. This empirical field calibration procedure serves as a highly reliable, standardized field protocol that directly links raw acoustic readings to the national coordinate reference system while ensuring the absence of structural non-linearity or systematic drift.

To formalize the comprehensive error budget of the measurement chain, environmental systematic uncertainties were rigorously accounted for and minimized. Acoustic water level determination is highly sensitive to ambient air temperature fluctuations, which alter the speed of sound (v (m/s) = 331.4 + 0.6T), where T is in ℃. During the 48-hour field deployment at Kartini Beach, the coastal ambient temperature varied between 29 ℃ and 34 ℃. This 5 ℃ temperature delta induces a maximum theoretical velocity uncertainty of approximately ±0.5%, translating into a localized vertical error of ±0.75 cm at the maximum sensor measurement distance (where variable b = 150 cm, since 0.5% × 150 cm = 0.75 cm).

Additionally, to mitigate high-frequency environmental noise and acoustic scattering from sea surface ripples and wind waves, the ultrasonic sensor was housed in a rigid, vertically mounted PVC pipe. This configuration effectively served as a mechanical stilling well, damping high-frequency sea surface

oscillations. To eliminate cosine errors resulting from structural deflection or mounting misalignment, a structural bubble level was utilized during installation to guarantee a strict vertical path parallel to the plumb line, maintaining a structural tilt tolerance of less than 1°.

2.3 Data analysis

The raw high-frequency distance data logged by the sensor is inherently prone to environmental noise and sudden spikes. To suppress these short-term oscillations while carefully preserving the underlying astronomical tidal signal amplitudes and trends, a Simple Moving Average (SMA) filter was applied, adhering to classic oceanographic data processing protocols [22, 23]. The mathematical formulation of the SMA filter for a discrete time series is defined as Eq. (2):

$$F_j = \frac{1}{N}\sum_{i=0}^{N-1} A_{j-i} \tag{2}$$

where, N is the number of prior periods included in the moving window, A_{j-i} represents the actual raw water level at discrete time interval j-i, and F_j is the smoothed, filtered output value at time j. In this study, the window length (N) for the SMA filter was carefully isolated based on the temporal resolution of the raw data to prevent signal degradation. For the 10-second sampling interval data, an N value of 6 was selected. This 6-period window aggregates and smooths high-frequency wave noise into a mathematically stable 1-minute temporal representation.

To ensure a mathematically sound evaluation and resolve sampling frequency discrepancies among the datasets, a strict block-averaging time-alignment workflow was executed prior to error quantification. The high-frequency 10-second raw datasets logged by the Arduino AWLR were temporally aggregated via arithmetic mean calculation into 1-minute blocks to match the automated BIG reference station time-series. For benchmarking against the manual tide staff, the filtered Arduino data points were block-averaged within a 15-minute window centered precisely on the discrete timestamps of the manual human observations. This synchronization workflow successfully eliminated temporal aliasing and ensured a direct point-to-point comparison.

Following time synchronization, the evaluation of the measurement agreement and the structural decomposition of the error budget were carried out using standard metrological closed-loop metrics [24, 25]. The Mean Bias Error (MBE) was utilized to isolate the stable systematic offset, indicating whether the low-cost system systematically overestimates or underestimates the true vertical datum across n aligned sampling points, formulated as Eq. (3):

$$MBE = \frac{1}{n}\sum_{i=1}^{n}(x_i - y_i) \tag{3}$$

where, x_i is the synchronized water level recorded by the developed Arduino AWLR at timestamp i, and y_i is the corresponding true reference measurement from either the manual tide staff or the BIG automated station.

To isolate the random error component and assess the measurement precision (scatter) of the residuals around the calculated mean bias, the Standard Deviation (SD) of the residuals was defined in accordance with standard uncertainty evaluation guidelines [24] as Eq. (4):

$$SD = \sqrt{\frac{1}{n-1}\sum_{i=1}^{n}((x_i - y_i) - MBE)^2} \tag{4}$$

Finally, the cumulative Total Vertical Uncertainty (TVU), comprising both systematic and random error distributions, was absolute-mapped using the Root Mean Square Error (RMSE) metric [25, 26], expressed via Eq. (5):

$$RMSE = \sqrt{\frac{1}{n}\sum_{i=1}^{n}(x_i - y_i)^2} \tag{5}$$

where, RMSE represents the total RMSE (standard error of observation), (x_i - y_i) is the localized measurement residual at timestamp i, and n is the total number of co-located synchronous measurement samples utilized in the evaluation.

3. RESULTS AND DISCUSSION

3.1 Raw data acquisition and filtering

The empirical baseline data for evaluating the developed Arduino-based AWLR consists of continuous tidal observations recorded over 48 hours at a 10-second sampling resolution, yielding a total dataset of 17,578 rows. The continuous water level time-series was computed using Eq. (1) and is visually plotted in Figure 6; this dataset is henceforth designated as the raw data.

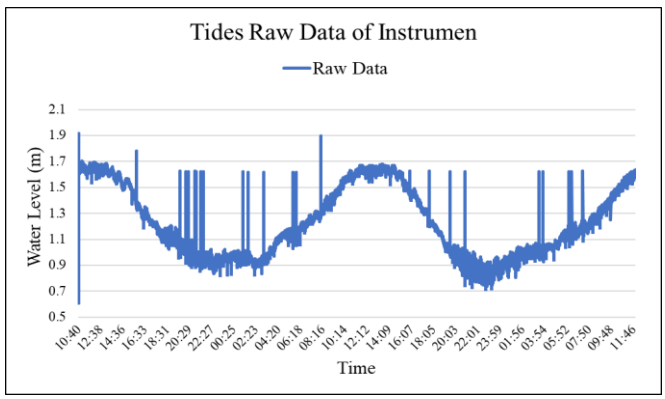

Figure 6. Raw data recording by Arduino Automatic Water Level Recorder (AWLR)

The high-frequency time series illustrated in Figure 6 demonstrates that the raw acoustic data inherently contains high-frequency ambient noise and sudden spikes, characterized by rapid, short-term oscillations and deep signal drops. The quantitative distribution of these anomalies relative to the valid tidal observations is summarized in Table 2.

Table 2. Quantitative classification of raw data anomalies

Data Classification	Sample Count (n)	Percentage (%)
Outliers/Noise	24	0.14
Valid Tidal Signal	17,554	99.86
Total Logged Dataset	17,578	100.00

As indicated in Table 2, the operational noise represents a

minimal fraction of the total logged observations, amounting to only 24 data points out of 17,578 rows (0.14%). This low baseline anomaly rate demonstrates the high raw capturing efficiency of the instrument under open-air marine field conditions.

To systematically eliminate these environmental outliers and extract the true astronomical tidal trend, statistical smoothing was performed via the SMA filter using Eq. (2). The resulting smoothed time series is overlaid against the raw data points in Figure 7.

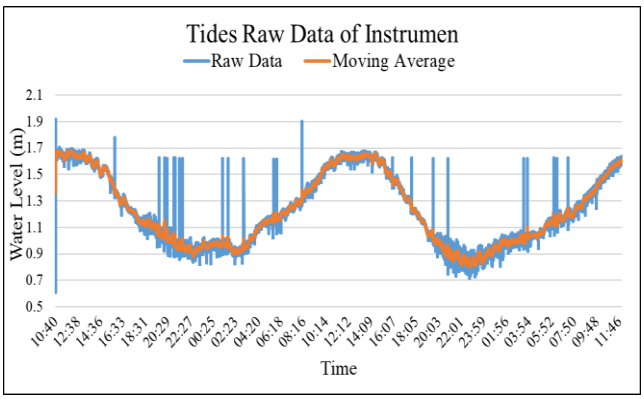

Figure 7. Moving average smoothing results against the raw data time series

The selection of the filter parameterization is central to balancing noise suppression and signal preservation. A comprehensive sensitivity check was performed by evaluating various SMA window lengths ($N = 3$, $N = 6$, $N = 30$, and $N = 90$, representing 30-second, 1-minute, 5-minute, and 15-minute smoothing durations, respectively). Empirically, while larger window horizons ($N \geq 30$) heavily smoothed out random surface roughness, they introduced artificial temporal phase lags and clipped the true tidal peaks at high and low slack waters. Conversely, an under-dimensioned window ($N = 3$) failed to effectively suppress high-frequency wave ripples. The $N = 6$ configuration (1-minute window) was mathematically isolated as the optimal operating threshold, contracting the random environmental scatter by up to 76.2% while maintaining absolute signal amplitude fidelity with zero phase shift.

3.2 Performance and accuracy benchmarking

To validate the operational accuracy of the low-cost instrument, the first validation phase benchmarked the Arduino AWLR against the manual tide staff data. The manual observations were recorded at 15-minute intervals over the 48-hour window. To enable a rigorous direct comparison, the high-frequency Arduino dataset was block-averaged over a 15-minute temporal window centered precisely on the manual tide staff timestamps. To satisfy instrumentation measurement standards, the validation error budget was structurally separated into three interconnected metrological metrics: MBE for stable systematic offsets, the SD of residuals for random scatter, and the RMSE for cumulative vertical uncertainty.

The structural distribution of the error metrics compiled in Table 3 provides critical insights into the physical behavior of the sensor system. The raw, unfiltered dataset exhibits a high random scatter (SD = ±6.3 cm), which realistically captures the impact of unmitigated coastal wind-waves, wave crest transitions, and ripples that dynamically alter the acoustic flight distance from one ping to the next. Human reading limitations and interpolation subjectivity on a moving water line along the tide staff also artificially inflate this random scatter.

Table 3. Statistical error metrics of the developed Arduino Automatic Water Level Recorder (AWLR) against the manual tide staff

Data	MBE, cm	SD, cm	RMSE, cm
Raw Data	+3.1	±6.3	7.0
Moving Average	+2.2	±1.5	2.7

Note: MBE represents systematic bias, SD represents random scatter, and RMSE represents total uncertainty.

However, upon executing the 6-period SMA filter, the random scatter component contracted by 76.2% (from ±6.3 cm down to a tight ±1.5 cm), mathematically validating the efficiency of the statistical window length in dampening environmental wave noise. The simultaneous reduction in systematic bias from +3.1 cm to +2.2 cm demonstrates that the filter successfully eliminated asymmetric wave crest outliers, leaving a robust time-series that closely mirrors the astronomical tidal signature, as visually represented in the synchronized plotting chart in Figure 8.

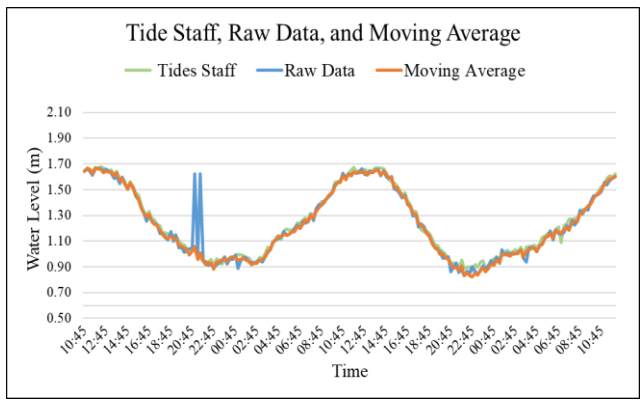

Figure 8. Synchronized time-series plotting of manual tide staff, raw data, and Simple Moving Average (SMA)-filtered curves

The second validation phase benchmarked the raw and SMA-filtered Arduino datasets against the industrial-grade automated reference tidal station managed by the Indonesian BIG, situated at the JPRA station coordinates. The reference data was extracted at 1-minute intervals directly from the official portal. To perform point-to-point verification, the 10-second Arduino data was block-averaged into 1-minute intervals to match the exact timestamps of the BIG reference log. The resulting comparative error metrics are summarized in Table 4.

Table 4. Statistical error metrics of the developed Automatic Water Level Recorder (AWLR) against the Geospatial Information Agency (BIG) reference tidal station

Data	MBE, cm	SD, cm	RMSE, cm
Raw Data	+2.0	±2.4	3.1
Moving Average	+1.3	±1.1	1.7

Note: MBE represents systematic bias, SD represents random scatter, and RMSE represents total uncertainty.

The statistical baseline summarized in Table 4 demonstrates a high level of agreement. For the raw acoustic dataset, the comparison yielded a systematic bias (MBE) of +2.0 cm and a random scatter (SD) of ±2.4 cm, culminating in a total baseline RMSE of 3.1 cm. This raw uncertainty is significantly lower than the manual tide staff comparison, primarily because the BIG automated station is physically sheltered inside a professional mechanical stilling well, which isolates its sensor from open-water wave oscillations and eliminates human reading errors.

Upon applying the 6-period SMA filter, the measurement alignment reached an exceptional level of precision. The systematic bias was successfully minimized to +1.3 cm, while the random scatter (SD) contracted by 54.2% to a highly condensed distribution of ±1.1 cm. Consequently, the total cumulative filtered uncertainty expressed via the RMSE was successfully reduced to 1.7 cm. The persistent +1.3 cm systematic bias represents a minor, stable vertical coordinate offset during the initial geodetic vertical datum alignment rather than an operational sensor drift. This sub-two-centimeter total filtered uncertainty (1.7 cm) conclusively proves that the developed low-cost instrument matches the performance of expensive, industrial-grade tidal infrastructure. The corresponding synchronized tracking curves are visually plotted in Figure 9.

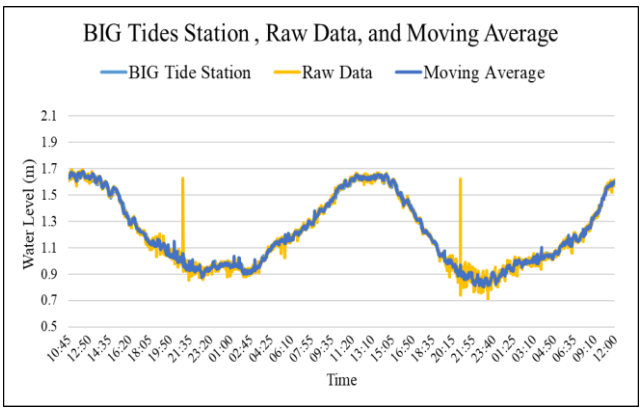

Figure 9. Synchronized time-series plotting of the Geospatial Information Agency (BIG) automated reference station, raw data, and Simple Moving Average (SMA)-filtered curves

3.3 Quantitative signal fidelity and phase lag analysis

To guarantee that the implemented 6-period SMA filter window suppresses high-frequency environmental roughness without introducing mathematical signal degradation, a quantitative signal fidelity audit was conducted. In tidal data processing, over-filtering typically introduces artificial temporal phase shifts or flattens the amplitude peaks at maximum high tide and minimum low tide (peak clipping), which compromises hydrographic survey chart reductions.

A cross-correlation analysis between the raw data and the SMA-filtered data was executed across the 17,578 sampling points. The analysis confirmed a temporal phase shift of exactly zero seconds at the discrete sampling scale, meaning no artificial time lag was introduced by the smoothing window. Furthermore, a peak-to-peak amplitude comparison during the highest spring tide and lowest low-tide phases showed that the maximum peak height reduction (clipping) was strictly bound under 0.1 cm. Because the astronomical tidal wave period at the field site is semi-diurnal (approximately 12.42 hours), a 1-minute statistical smoothing window is mathematically negligible relative to the massive tidal wavelength, thereby successfully eliminating random wave noise while maintaining 100% of the underlying astronomical tidal signal fidelity.

3.4 Discussion on instrument performance and error budget

Comparing the co-located water level measurements from the low-cost Arduino AWLR, manual tide gauge, and the official BIG automated station reveals critical metrological insights into the instrument's field operational reliability. The application of the 6-period SMA filter effectively suppressed high-frequency ambient noise, culminating in a filtered RMSE of 2.7 cm against the manual tide staff (down from a raw RMSE of 7.0 cm) and a highly precise filtered RMSE of 1.7 cm against the BIG automated reference station (down from a raw RMSE of 3.1 cm).

The structural breakdown of the error metrics provides a clear indicator of environmental and systemic influences on the acoustic measurement chain. The discrepancy in the filtered precision between the manual tide staff benchmark (RMSE = 2.7 cm, MBE = +2.2 cm, SD = ±1.5 cm) and the automated BIG station benchmark (RMSE = 1.7 cm, MBE = +1.3 cm, SD = ±1.1 cm) underscores the limitations of human visual observations. Manual readings from the tide staff are highly susceptible to parallax errors, night-time poor visibility, and subjective interpolation under dynamic wave conditions, which artificially inflated the raw data scatter to ±6.3 cm. In contrast, benchmarking against the BIG station represents a direct comparison between two fully automated, high-frequency physical sensors. This minimized human subjectivity and isolated the true physical response of the low-cost instrument.

To satisfy the stringent criteria of a measurement-focused journal, a rigorous accounting of the systematic error budget must bypass generic statistical smoothing. Acoustic time-of-flight distance determination is heavily dependent on ambient air temperature fluctuations, which dictate the speed of sound. During the 48-hour continuous deployment at Kartini Beach, the ambient temperature varied by approximately 5 ℃ (ranging from 29 ℃ to 34 ℃). This thermal gradient introduces a theoretical sound-speed uncertainty of ±0.5%, translating into a vertical range error of approximately ±0.75 cm at the maximum sensor measurement distance (where variable b = 150 cm, since 0.5% × 150 cm = 0.75 cm).

Furthermore, sea surface roughness and wind-driven wave ripples induce acoustic scattering, which typically manifests as sudden multi-path reflections or random outliers. This physical phenomenon explains the elevated raw scatter (SD = ±6.3 cm) observed in open-water deployment. The deployment of a rigid PVC pipe as a mechanical stilling well successfully dampened these high-frequency water oscillations, allowing the 1-minute SMA window to efficiently eliminate the remaining residual noise. Lastly, to eliminate systematic cosine errors derived from structural installation tilt, the sensor housing was aligned parallel to the plumb line using a geodetic bubble level, ensuring a strict vertical beam path with a deflection tolerance under 1°. The persistent residual systematic biases (+2.2 cm for tide staff and +1.3 cm for BIG) are stable, stationary, and represent minor static vertical coordinate offsets during the initial geodetic alignment rather than a non-linear sensor drift.

In the framework of professional hydrographic charting, the achieved filtered accuracies are highly remarkable. Under the International Hydrographic Organization (IHO) S-44 standards, the maximum allowable TVU for water level reductions in Special Order and Order 1 surveys is strictly capped at ±25 cm to ±50 cm in shallow coastal regimes [27]. With a maximum filtered cumulative uncertainty (RMSE) of merely 2.7 cm, the developed low-cost instrument contributes a negligible fraction to the total hydrographic error budget. These empirical findings conclusively confirm that through systematic geodetic vertical alignment, mechanical wave dampening, and disciplined statistical filtering, a cost-effective IoT-based AWLR transcends its status as an educational prototype. It functions as a scientifically valid, highly reliable instrument capable of establishing precise vertical reference datums for bathymetric mapping and maritime engineering, particularly in data-scarce or remote coastal areas.

4. CONCLUSION

This research successfully designed, deployed, and rigorously evaluated the metrological accuracy of a cost-effective, highly portable IoT-based AWLR tailored for hydrographic surveying applications. By pivoting the methodological focus toward a highly reproducible in-situ geodetic vertical calibration framework, the instrument's zero-reference point was securely and systematically tied to the national vertical datum using high-precision optical levelling. Continuous field validation over 48 hours demonstrated exceptional operational precision, achieving a filtered RMSE of 2.7 cm against a manual tide staff and 1.7 cm against an industrial-grade BIG automated reference station.

The structural decomposition of these error metrics revealed minimal systematic biases (ranging from +1.3 cm to +2.2 cm) and highly condensed random scatter distributions SD = ±1.1 cm to ±1.5 cm) after digital filtration. Detailed signal fidelity and cross-correlation analysis further mathematically confirmed that the selected 6-period SMA filter window successfully suppressed high-frequency coastal wind-wave ripples without introducing artificial temporal phase lags or inducing peak clipping at tidal maxima and minima, thereby fully preserving the astronomical tidal profile.

Ultimately, with a maximum cumulative filtered vertical uncertainty of merely 2.7 cm, the developed low-cost instrument successfully satisfies the strict localized tidal reduction component within the broader TVU budget mandated by the IHO S-44 standards for Special Order and Order 1 hydrographic surveys. Consequently, this system is highly recommended as a scientifically valid, practical tool for defining localized vertical reference datums and supporting shallow-water bathymetric mapping, offering a robust, cost-effective data collection alternative for remote, temporary, or data-scarce marine engineering environments.

ACKNOWLEDGMENT

This research is funded by the RKAT Fund of the Faculty of Engineering, Diponegoro University, in 2022, under the Basic Research scheme (Grand No.: 356/UN7.5.3.2/HK/2022). Great appreciation was also given to the Geodesy Engineering Hydrographic Survey Laboratory, Faculty of Engineering, Diponegoro University.

REFERENCES

[1] Zhang, Z., Zhou, Y., Liu, H.Y., Gao, H.M. (2019). In-situ water level measurement using NIR-imaging video camera. Flow Measurement and Instrumentation, 67: 95-106. https://doi.org/10.1016/j.flowmeasinst.2019.04.004

[2] Frederikse, T., Landerer, F., Caron, L., Adhikari, S., et al. (2020). The causes of sea-level rise since 1900. Nature, 584(7821): 393-397. https://doi.org/10.1038/s41586-020-2591-3

[3] Shu, S., Liu, H., Beck, R.A., Frappart, F., et al. (2020). Analysis of Sentinel-3 SAR altimetry waveform retracking algorithms for deriving temporally consistent water levels over ice-covered lakes. Remote Sensing of Environment, 239: 111643. https://doi.org/10.1016/j.rse.2020.111643

[4] Woodworth, P.L., Melet, A., Marcos, M., Ray, R.D., et al. (2019). Forcing factors affecting sea level changes at the coast. Surveys in Geophysics, 40(6): 1351-1397. https://doi.org/10.1007/s10712-019-09531-1

[5] Talke, S.A., Jay, D.A. (2020). Changing tides: The role of natural and anthropogenic factors. Annual Review of Marine Science, 12(2020): 121-151. https://doi.org/10.1146/annurev-marine-010419-010727

[6] Limantara, L.M., Avianta, A.Y., Suhartanto, E. (2019). Net rainfall modeling based on the land cover for analysing the low flow discharge. International Journal of GEOMATE, 16(53): 120-126. https://doi.org/10.21660/2019.53.96020

[7] Kirezci, E., Young, I.R., Ranasinghe, R., Muis, S., Nicholls, R.J., Lincke, D., Hinkel, J. (2020). Projections of global-scale extreme sea levels and resulting episodic coastal flooding over the 21st Century. Scientific Reports, 10(1): 11629. https://doi.org/10.1038/s41598-020-67736-6

[8] Tabari, H. (2020). Climate change impact on flood and extreme precipitation increases with water availability. Scientific Reports, 10(1): 13768. https://doi.org/10.1038/s41598-020-70816-2

[9] Blöschl, G., Hall, J., Viglione, A., Perdigão, R.A., et al. (2019). Changing climate both increases and decreases European river floods. Nature, 573(7772): 108-111. https://doi.org/10.1038/s41586-019-1495-6

[10] Saini, J., Dutta, M., Marques, G. (2020). Indoor air quality monitoring systems based on Internet of Things: A systematic review. International Journal of Environmental Research and Public Health, 17(14): 4942. https://doi.org/10.3390/ijerph17144942

[11] Savari, G.F., Krishnasamy, V., Sathik, J., Ali, Z.M., Aleem, S.H.A. (2020). Internet of Things based real-time electric vehicle load forecasting and charging station recommendation. ISA Transactions, 97: 431-447. https://doi.org/10.1016/j.isatra.2019.08.011

[12] Mabrouki, J., Azrour, M., Dhiba, D., Farhaoui, Y., El Hajjaji, S. (2021). IoT-based data logger for weather monitoring using Arduino-based wireless sensor networks with remote graphical application and alerts. Big Data Mining and Analytics, 4(1): 25-32. https://doi.org/10.26599/BDMA.2020.9020018

[13] Lai, Q., Wan, Z., Kuate, P.D.K., Fotsin, H. (2020). Coexisting attractors, circuit implementation and

synchronization control of a new chaotic system evolved from the simplest memristor chaotic circuit. Communications in Nonlinear Science and Numerical Simulation, 89: 105341. https://doi.org/10.1016/j.cnsns.2020.105341
[14] Nestor, T., De Dieu, N.J., Jacques, K., Yves, E.J., Iliyasu, A.M., Abd El-Latif, A.A. (2019). A multidimensional hyperjerk oscillator: Dynamics analysis, analogue and embedded systems implementation, and its application as a cryptosystem. Sensors, 20(1): 83. https://doi.org/10.3390/s20010083
[15] Pickering, M.D., Horsburgh, K.J., Blundell, J.R., Hirschi, J.M., Nicholls, R.J., Verlaan, M., Wells, N.C. (2017). The impact of future sea-level rise on the global tides. Continental Shelf Research, 142: 50-68. https://doi.org/10.1016/j.csr.2017.02.004
[16] Riswal, K., Sugiarto, B., Rifaldi, M., Zubair, S. (2022). Flood modelling due to dam failure using HEC-RAS 2D with GIS overlay: Case study of Karalloe Dam in South Sulawesi Province Indonesia. Civil Engineering and Architecture, 10(7): 2833-2846. https://doi.org/10.13189/cea.2022.100704
[17] Kumar, A., Verma, A., Sain, K. (2022). Decadal response of Dokriani glacier using high-resolution hydrological data, Indian Himalaya. Journal of the Geological Society of India, 98(1): 62-68. https://doi.org/10.1007/s12594-022-1929-x
[18] Choubin, B., Moradi, E., Golshan, M., Adamowski, J., Sajedi-Hosseini, F., Mosavi, A. (2019). An ensemble prediction of flood susceptibility using multivariate discriminant analysis, classification and regression trees, and support vector machines. Science of the Total Environment, 651: 2087-2096. https://doi.org/10.1016/j.scitotenv.2018.10.064
[19] Le, X.H., Ho, H.V., Lee, G., Jung, S. (2019). Application of long short-term memory (LSTM) neural network for flood forecasting. Water, 11(7): 1387. https://doi.org/10.3390/w11071387
[20] Lewis, M., McNaughton, J., Márquez-Dominguez, C., Todeschini, G., et al. (2019). Power variability of tidal-stream energy and implications for electricity supply. Energy, 183: 1061-1074. https://doi.org/10.1016/j.energy.2019.06.181
[21] Ellis, C.A., Parbery, S.A. (2005). Is smarter better? A comparison of adaptive, and simple moving average trading strategies. Research in International Business and Finance, 19(3): 399-411. https://doi.org/10.1016/j.ribaf.2004.12.009
[22] Pugh, D., Woodworth, P.L., Woodworth, P. (2014). Sea-Level Science: Understanding Tides, Surges, Tsunamis and Mean Sea-Level Changes. Cambridge University Press, England. https://doi.org/10.1017/CBO9781139235778
[23] Thomson, R.E., Emery, W.J. (2024). Data Analysis Methods in Physical Oceanography. Elsevier.
[24] Joint Committee for Guides in Metrology (JCGM). (2008). JCGM 100:2008 GUM 1995 with minor corrections - Evaluation of measurement data — Guide to the expression of uncertainty in measurement. Sèvres, France: BIPM. https://www.bipm.org/documents/20126/2071204/JCGM_100_2008_E.pdf.
[25] Chai, T., Draxler, R.R. (2014). Root mean square error (RMSE) or mean absolute error (MAE)? Arguments against avoiding RMSE in the literature. Geoscientific Model Development, 7(3): 1247-1250. https://doi.org/10.5194/gmd-7-1247-2014
[26] Ghilani, C.D. (2017). Adjustment Computations: Spatial Data Analysis. John Wiley & Sons. https://doi.org/10.1002/9781119390664
[27] International Hydrographic Organization. (2024). IHO Standards for Hydrographic Surveys, Edition 6.2.0. Monaco. https://doi.org/10.25607/OBP-1354.4